

Optical absorption edge shifts in electrodeposited ZnO thin films

Tingting Ren, Holly R. Baker and Kristin M. Poduska *

*Department of Physics and Physical Oceanography, Memorial University of
Newfoundland, St. John's, NL A1B 3X7 Canada*

Abstract

Electrodeposited wurtzite ZnO thin films exhibit shifts in their optical absorption edges with changes in thickness (0.2 – 2 μm), deposition potential (-0.80 V to -1.50 V), and aging time (days to months under ambient conditions). Increases in absorption edge energy are consistent with H^+ incorporation as a shallow donor (Burstein-Moss effect) due to deposition in the presence of electrochemically evolved hydrogen. Diffuse reflectance spectroscopic data and Raman spectroscopic data show both potential- and thickness-dependent changes in defect levels and absorption edges, which suggests that H^+ can be trapped in secondary defects. Such defects also increase the diffusion time for H^+ and lead to the observed decay in absorption edge energy with aging.

Key words: Zinc oxide, Electrochemistry, Optical properties, X-ray diffraction, Reflection spectroscopy, Raman scattering, Hydrogen, Diffusion

* Phone: 709.737.8890, Fax: 709.737.8739

Email address: tingting@physics.mun.ca, holly.r.baker@gmail.com,
kris@physics.mun.ca (Tingting Ren, Holly R. Baker and Kristin M. Poduska).

1 Introduction

Tailored optical responses of semiconductor materials lie at the heart of multi-billion dollar industries, including thin film transistor-based devices and photovoltaic cells [1]. As an economical alternative to ultrahigh vacuum-based deposition methods, electrodeposition is showing promise for preparing thin film materials and devices for photovoltaic applications [2,3]. A key to implementing electrodeposition in these technologies is the ability to control the defects and dopants that affect a material's optical response.

Defect levels in materials are typically adjusted by balancing kinetic and thermodynamic growth. In electrodeposited materials, indirect evidence suggests that defect concentrations can be influenced by control of temperature[4,5] as well as applied deposition potential [6,7]. Doping can be controlled by using ultrapure solutions and reagents, and purging the electrolyte with an inert gas such as argon before and during deposition, thus limiting the types and amounts of foreign ions present in the electrolyte during deposition [3,8].

While many dopants can be detected even in relatively small amounts, hydrogen incorporants are more elusive, but still very important to consider in ZnO prepared by any method. In the vast majority of semiconducting materials, hydrogen species are amphoteric inclusions and neither contribute to electron conduction nor affect a material's optical band gap [9]. However, both theoretical studies [10] and experiments on thin films prepared by other methods [11,12] have shown that hydrogen incorporation into ZnO leads to *n*-type doping. These hydrogen donors occupy levels within the conduction band, thereby increasing the magnitude of the band gap energy (Burstein-Moss effect) [13].

Since hydrogen is present in many different methods of ZnO synthesis, including vapour-phase transport, hydrothermal growth, and metal-organic chemical vapour deposition, even samples which have not been intentionally doped will be affected by hydrogen inclusions.

Electrodeposition is not immune to issues of hydrogen incorporation. The two most common approaches to ZnO electrodeposition use reduction of ambient oxygen or nitrate ions in the presence of Zn^{2+} to trigger an electroprecipitation reaction [14]. Since water is not stable at the potentials at which appreciable ZnO deposition occurs, hydrogen gas is evolved directly at the working electrode (substrate) surface. Despite the relatively large amount of hydrogen evolved during ZnO electrodeposition (30% – 70% of the total current) [15], it would appear that unusually large amounts of hydrogen are not incorporated in ZnO electrodeposits, since there are many reports of optical band gaps in such films that agree well with bulk values [6,7,16,17].

A move toward tuning optical band gaps of electrodeposited ZnO thin films has been initiated by several groups over the past decade. Differences have been observed in the absorption edge of native electrodeposited ZnO (no intentional dopants) with parameters such as deposit thickness, crystallite size, deposition potential, electrolyte composition, and *in situ* or *ex situ* heat treatments [4–7,17]. However, there has been surprisingly little attention paid to understanding why these parameters influence the optical absorption edge. One recent study attributes shifts in the absorption edge of electrodeposited ZnO films prepared at different temperatures to quantum confinement effects resulting from a large dispersion in crystallite sizes [5]. The data that we present in this work suggest that factors other than quantum confinement are responsible for absorption edge shifts in our electrodeposited films.

The present study was designed to investigate factors that occur during the normal course of ZnO electrodeposition which affect the optical absorption edge. While confirming earlier reports of changes in optical band gap with thickness [7], we also observe variations with deposition potential which do not result from changes in lattice parameters, unlike earlier reports [6,7]. These absorption edge changes are discussed in the context of deposition in the presence of electrochemically evolved hydrogen, average crystallite sizes, and hydrogen diffusion with sample aging.

2 Experimental Details

2.1 Synthesis

We synthesized ZnO using an aqueous electrodeposition method first reported by Izaki and Omi [16] and whose mechanism was investigated more recently [15,18]. ZnO formation requires basic pH conditions, and this is achieved during electrodeposition by reduction of nitrate or oxygen at the working electrode surface to form a highly localized source of OH^- . In this study, a 0.01 M $\text{Zn}(\text{NO}_3)_2$ electrolyte served as the source of nitrate and zinc ions. This concentration is one order of magnitude lower than that used in earlier studies of relevance [5,7], in order to minimize the risk of forming secondary phases [14]. Electrolytes were thoroughly purged with argon before and during deposition to reduce the possibility of parallel OH^- production from oxygen reduction [14]. All electrolytes were prepared from ACS reagent grade salts (EM Scientific) and ultrapure water (Barnstead Nanopure, $18.2 \text{ M}\Omega\cdot\text{cm}$), with pH = 5.

Potentiostatic depositions (-0.70 V to -1.50 V) were carried out in a conventional three-electrode cell, with a gold wire counter electrode and an Ag/AgCl reference electrode. All potentials are reported with respect to Ag/AgCl. Depositions were carried out at 70°C to reduce the thermodynamic favorability of $\text{Zn}(\text{OH})_2$ formation [14]. Polycrystalline stainless steel working electrodes were pretreated by sanding with 1500 grit sand paper followed by five minutes of sonication in ultrapure water. Potential control during the experiments was maintained with a potentiostat (Hokuto Denko HA-501) and the charge passed during depositions was recorded with a coulombmeter (Hokuto Denko HF-201). Deposition currents and potentials were recorded and analyzed using LabVIEW (National Instruments) virtual instruments of our own design and modified from others [19]. Film thicknesses ranged from $0.2\text{--}2\ \mu\text{m}$, depending on deposition time and potential.

2.2 Characterization

Phase identification of the electrodeposits was possible through a combination of X-ray diffractometry (XRD), using a Rigaku RAC-C with Cu $K\alpha$ radiation, and Raman spectroscopy (LabRAM, Jobin Yvon Horiba, 532 nm). The former method provided unit cell parameters, crystallite size, and film texture information, while the latter yielded vibrational information specific to crystal structure and local chemical composition. Lattice constant refinements from XRD data, including refinement of zero shift offsets, were facilitated by the LATCON software package [20]. Average crystallite sizes were determined from XRD peak broadening data [4], using peaks widths from a silicon standard to correct for instrumental broadening effects. Deposit morphologies and

cross-sectional thicknesses were assessed with a scanning electron microscope (SEM) from Hitachi (S570, 20 keV). Thickness measurements were also confirmed with atomic force microscopy (Asylum Research MFP-3D).

Due to the opaque stainless steel substrates, optical transmission measurements were not feasible. Thus, UV-Vis diffuse reflectance spectroscopy, using an OceanOptics DT 1000 CE spectrophotometer in a 45 degree collection orientation, provided optical absorption edge data. From these data, the optical band gap can be assessed in two ways. First, the absorption edge corresponds approximately to the wavelength at which the reflectance increases above its minimum value. Second, the band gap corresponds to the peak of the first derivative of the reflectance versus wavelength plot. The former method applies rigorously only to transmission data, while the latter method applied rigorously only to samples with grain sizes of 10 μm or larger [21]. While both methods show consistent qualitative trends, these two approaches yield optical transitions which differ by as much as 10 nm (0.1 eV). Earlier reports have demonstrated that the derivative analysis yields band gap values which are closer to the true values obtained from transmission measurements [7]. Therefore, we use results from the derivative method for quantitative comparisons.

3 Results

XRD data show that electrodeposits prepared at a constant potential between -0.80 V and -1.40 V are strongly textured, phase-pure wurtzite ZnO (Figure 1a). All observed Bragg reflections are consistent with wurtzite's $P6_3mc$ space group, with the (002) reflection dominant in all deposits. Lattice constant refinements for electrodeposits of all thicknesses, prepared over the entire po-

tential range, yield an hexagonal unit cell which compares favorably with the accepted bulk unit cell parameters of $a = 3.250 \text{ \AA}$ and $c = 5.207 \text{ \AA}$ (JCPDS 36-1451) [22], as shown in Figure 1b. Within uncertainty estimates, the c/a ratios show little change with deposition potential or film thickness (Figure 1c). Others have reported lattice constant changes of up to 0.02 \AA with film thickness [7], as well c/a ratios that increase with increasing deposit thickness [7] or more negative deposition potentials [6]. These changes were attributed to dopant incorporation or stress. Energy dispersive X-ray analyses on our electrodeposits show no sign of impurities with masses heavier than sodium.

SEM images of crystallite morphologies in the electrodeposits are consistent with the preferred orientation trends observed in the XRD data. Figure 2 shows hexagonal rod-like growth habits for deposits prepared at potentials more positive than -1.20 V . This rod-like growth continues over time, with rod height increasing first, followed by a period of slightly preferential radial growth (Figure 2a-c). This trend is confirmed by comparing deposit thickness with charge passed during deposition, as presented in Figure 3. The slope of the thickness *vs.* charge trend is shallower for more positive deposition potentials, while deposits prepared at potentials $\leq -1.10 \text{ V}$ show a steeper slope.

An explanation for the potential-dependent transition in the thickness *versus* charge trend involves changes in crystallite growth morphologies. At more negative potentials, the hexagonal rod growth is accompanied by “twin-rice” $(000\bar{1})$ - $(000\bar{1})$ bicrystallite growth on top of a dense, textured underlayer (Figure 2d-f). The elongated bicrystallite growth mode, based on inversion boundaries, has been observed in ZnO prepared by other methods [23].

While thickness and morphological differences do not appear to influence the

average lattice parameters of the ZnO electrodeposits, both of these factors affect their optical absorption edges. At a given deposition potential, the energy of the absorption edge decreases with increasing film thickness, as shown in Figure 4 and Figure 5, consistent with earlier reports in thicker (1–30 μm) electrodeposited films [7]. The shape of the transitions are very similar among deposits prepared at the same potential, even for different thicknesses. However, there is a tendency towards broader peak widths for samples prepared at more negative potentials. This suggests that similar types of defects are likely present in samples prepared at the same potential, regardless of thickness. Wider transitions are generally indicative of more dispersion in crystallite sizes and/or defect levels [24].

The maximum diffuse reflectance intensity depends largely on deposit roughness, rather than deposit thickness. This is directly related to the differences in growth morphologies for deposits prepared at different potentials. For films with the columnar morphology ($E_{\text{applied}} \geq -1.10$ V), roughness tends to decrease with deposition time as radial growth fills in voids in the film, leading to more specular reflection and less diffuse reflection (Figure 4a). For films comprised of the dense underlayer and biaxial crystallites ($E_{\text{applied}} < -1.10$ V), the films grow rougher with time, leading to less specular reflection and more diffuse reflection (Figure 4b).

Figure 5 shows that both thickness and deposition potential affect the optical absorption edge of ZnO electrodeposits. The typical bulk value is 3.33 eV, as indicated by the dotted line [1]. While it is clear that the energy of the optical absorption edge decreases with increasing film thickness, its dependence on deposition potential is more complicated. For example, films with thicknesses in the range of 0.5 to 1.0 μm exhibit an absorption edge energy that increases

as the deposition potential is changed from -0.90 to -1.10 V. However, for deposition potentials more negative than -1.10 V, the absorption edge energy is significant lower. Thicker films (1.5 - 2.5 μm) do not show a clear trend in absorption energy with deposition potential, according to the data in Figure 5 and those from other films we have prepared (not shown). As a result, we focused subsequent comparisons among films of comparable thickness, in the range of $0.5 - 1.0$ μm , in order to better understand the role of deposition potential on optical absorption edge. Our investigations are described in detail in the Discussion section below. The importance of thickness and deposition potential in tuning the optical responses of thin film ZnO has also been recognized by others [7,25].

We also observe that optical absorption edges of our ZnO electrodeposits tend to move to lower energy upon aging. The absorption edge decreases by ~ 0.05 eV within the first 48 hours, and can shift by ~ 0.1 eV over a span of weeks, as shown in Figure 6. The decay time of the absorption edge energy does not vary significantly with deposit thickness or deposition potential. Changes in electronic and spectroscopic properties with sample aging on the scale of days to weeks have been observed in ZnO prepared by other methods [26–28], but have not been reported for electrodeposited ZnO films.

4 Discussion

Changes in the absorption edge of thin film materials have been attributed to a range of factors, including quantum confinement [5,29], stress/strain [7], doping [1], and defects [30].

Electronic quantum confinement effects appear in crystallites whose sizes approach the exciton radius (~ 2 nm for ZnO) [1]. Optical confinement effects have been observed recently in quantum dots which are an order of magnitude larger [29]. In our ZnO electrodeposits, the absorption edge energies display no obvious dependence on average crystallite size. Data in Table 1 show that there is very little variation in average crystallite size with thickness or deposition potential, despite the spread in band gap energies. Marotti *et al.* [5] reported that electrodeposited ZnO band gap energies vary inversely with average crystal size, and that crystal size dispersion is also important. They report that 90% crystal size dispersion induces ~ 0.005 eV band gap energy increase in ZnO crystallites with average sizes of 45 – 50 nm. However, the band gap energy differences we observe in our films show much larger changes (0.25 eV) for a similar range of average crystallite sizes. This suggests that the crystal size dispersion effect does not affect the band gap energy as much as the film thickness and the applied potential do. Therefore, quantum confinement effects are not the dominant reason for the absorption edge changes in our electrodeposited ZnO films.

Stress and strain effects are unlikely to be large contributors either, as the lattice constant refinements show no appreciable change with different deposition potentials or sample thicknesses, in contrast to what others have observed [6,7]. Similarly, Raman spectroscopic data (discussed below) do not show peak shifts, a signature of stress or strain [31,32]. We conclude that the absorption edge changes in our electrodeposits result from electronic effects – rather than stress/strain effects – of doping and/or defects.

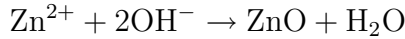
Unintentional native defects such as Zn and O vacancies or interstitials are most certainly present in our electrodeposits. However, recent theoretical stud-

ies of native point defects in ZnO have shown that those which are shallow donors (Zn interstitials or antisites) have high formation energies and are thus unlikely to contribute to the band gap shifts that we observe [33]. Other types of more probable native defects, including O vacancies, Zn vacancies, and O interstitials, are deep donors or acceptors and would not shift the optical absorption edge on their own accord.

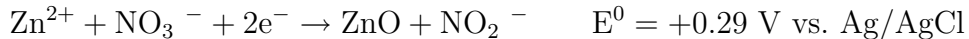
Our data suggest that dopants are likely the principle contributors to the band gap variations we observe. More specifically, hydrogen is a plausible dopant in our films based on the mechanism behind our electrodeposition method. ZnO formation in our experiments relies on nitrate reduction, as proposed and investigated by others [15,16].



Zinc ions and hydroxyl ions combine to form ZnO



to make the overall cathodic reaction



Previous studies have shown that ZnO growth via this mechanism is limited by kinetics, not mass transport, with the rate of ZnO formation increasing with more negative applied potentials [15]. Thus, even though the Nernst reversible potential for this reaction is +0.289 V, a large overpotential is required before appreciable ZnO electrodeposition occurs. We find very little deposit (0.1 μm thick or less) after 2 hours of deposition at potentials more positive than -0.80

V, consistent with earlier reports [15]. Therefore, we focused our studies on ZnO films prepared at potentials more negative than -0.80 V.

Since our window of interest is in a region of potential where water is not stable, hydrogen is also evolved during ZnO deposition.



The hydrogen evolution rate depends on pH and increases exponentially with a linear increase in applied overpotential. In our experiments, pH was held constant, so more negative deposition potentials led to more evolved hydrogen.

To quantify the relative importances of nitrate reduction, ZnO formation, and hydrogen evolution over our range of deposition potentials, we compared the charge produced in our working electrolyte with two reference electrolytes: a nitrate-containing electrolyte with no Zn (0.02 M KNO_3), and an electrolyte with neither Zn nor nitrate (0.02 M KCl). The concentrations of the reference electrolytes were chosen to match the anion concentration in the working electrolyte (0.02 M). Figure 7 shows the total amount of charge passed, during 10 minutes, in the three different electrolytes. In all electrolytes, the total amount of charge passed increases with more negative applied potentials. At more positive potentials (≥ -0.80 V), the charge passed in the two Zn-free electrolytes are similar and lower than in the Zn-containing electrolyte. This is consistent with the interpretations of Yoshida *et al.* who have indicated that zinc serves as a catalyst for nitrate reduction [15]. However, at more negative potentials, the two nitrate-containing electrolytes have similar current densities, both of which are higher than that for the chloride electrolyte. At potentials more negative than -1.30 V, hydrogen evolution is so vigorous that bubbles block

portions of the working electrode surface, making charge counting experiments unreliable.

If we make the simplistic assumption that the charge passed in the chloride electrolyte is due entirely to hydrogen evolution, and that the charge passed in the $\text{Zn}(\text{NO}_3)_2$ electrolyte is the sum of a potential-dependent hydrogen evolution current and nitrate reduction current, then the overall current efficiency for the ZnO formation is quite low ($\sim 30\%$) relative to that reported earlier for ZnO production at a stationary electrode ($\sim 70\%$) [15]. In terms of the absolute quantity of hydrogen evolved, if all evolved hydrogen were included into the ZnO electrodeposits, the stoichiometry would be 1:1 ZnO:H. However, we can safely assume that only a small portion of this hydrogen is actually incorporated, based on other studies that have related band gap shifts to carrier densities ($\sim 10^{19} \text{cm}^{-3}$) in ZnO [34,35]. Thus, hydrogen is present in excess during the ZnO electrodeposition process.

The hydrogen dopants that would cause a Moss-Burstein band gap shift are difficult to detect by bulk methods. Indeed, we see no significant change in lattice parameters as a function of film thickness or deposition potential, even though we do observe absorption edge shifts. The majority of studies that track hydrogen incorporation do so with spectroscopic methods [11,12,26,30,35] or gas effusion studies [12], and do not report lattice parameter data as a function of hydrogen incorporation levels. Therefore, we used Raman spectroscopy as a probe of local coordination environments to complement our bulk structural investigations.

Based on ZnO's wurzite-type structure, group theory predicts that Raman-active vibrational modes should include one A1 mode, two E2 modes, and

one E1 mode. In this case, the A1 and E1 modes are each polar, leading to a split into transverse optical (TO) and longitudinal optical (LO) modes.[36] The lower-frequency E2 mode is associated with the Zn sublattice, while the higher frequency E2 mode corresponds to the oxygen sublattice [29].

For our electrodeposited thin films, strong Raman transitions (Figure 8) were observed near 100 cm^{-1} (not shown) and 437 cm^{-1} , which can be assigned to E2(low) and E2(high), respectively [36]. The positions of these peaks did not shift with differences in deposition potential or deposit thickness, which suggests that there is neither significant stress nor significant changes in stress during film growth.

Other weaker Raman active modes were also observed. The A1(TO) mode is visible near 380 cm^{-1} . The broad peak near 580 cm^{-1} is consistent with recent reports of a LO quasimode, with mixed A1 and E1 symmetry, observed in poorly-oriented ZnO crystallite ensemble [37]. The broad peak visible near 330 cm^{-1} is attributed to a multiple phonon effect. At much higher wavenumbers ($2800\text{-}3000\text{ cm}^{-1}$, data not shown) where N-H, C-H, and O-H stretching modes would be visible [12], we see broad overlapping peaks which cannot be clearly resolved.

Relative decreases in the LO quasimode peak intensities occur with increasing film thickness (Figure 8a). The intensities of the A1(LO) and E1(LO) modes that contribute to this quasimode are reported to be enhanced by the presence of defects, in bulk crystals [30,38]. One possible explanation for the proportionally larger defect levels in thinner films is that the initial stages of ZnO film growth includes a higher defect level. Other work has shown the importance of a metallic Zn prelayer in the nucleation and growth of electrodeposited ZnO

[17], and our own studies of deposit morphologies during early stages of growth are consistent with this. Since the Zn prelayer is eventually converted to ZnO, this is a different growth mechanism than the Zn(OH)_2 precursor that has been reported for steady-state ZnO growth [15], and could result in a higher concentration of defects.

Relative decreases in the LO quasimode peak intensities also occur with more positive deposition potentials (Figure 8b). With more rapid deposition at more negative applied potentials, it is reasonable to expect higher defect concentrations.

The intensity enhancement in the LO quasimode with decreasing film thickness and more negative deposition potentials correlates with the blueshift of the optical absorption edge (Figure 4c). This suggests that higher defect concentrations contribute to higher energy absorption edges. However, unlike the diffuse reflectance data which show changes in the band gap with sample aging, there was no appreciable change in the relative intensities of the LO quasimode, or other Raman-active modes, with sample aging. This suggests that the absorption edge redshift with aging is not determined by the relative concentration of defects that contribute to the LO quasimode enhancement.

5 Conclusions

We propose that the potential-dependent absorption edge shifts observed in electrodeposited ZnO are due to a hydrogen-induced Burstein-Moss effect, and that the defects which lead to the LO quasimode enhancement are trapping sites for hydrogen to slow its diffusion. As shown earlier in Figure 5, the optical

absorption edges of all but the thickest of our electrodeposits were larger than those reported for bulk ZnO, consistent with hydrogen donors occupying levels within the conduction band to increase the magnitude of the band gap energy. Other studies have found monotonic increases in band gap with increasing H^+ levels in ZnO [35]. Carrier concentrations on the order of 10^{19} cm^{-3} are common for native ZnO, and increases in the carrier concentration by one order of magnitude can increase the optical band gap by 0.1 to 0.3 eV [34,35].

Recent theoretical studies have shown that hydrogen can diffuse readily in ZnO at ambient temperatures, but the presence of trapping sites provide a barrier to diffusion, even at temperatures well above room temperature [39]. Furthermore, hydrogen would need to be held at an electrically inactive trapping site for it to function as a donor. Applying these findings to the trends observed in our electrodeposited ZnO, we can arrive at several conclusions. First, hydrogen gas is present in excess during the electrodeposition process (as assessed from studies of charge passed during deposition, in Figure 7). Second, film thickness and deposition potential affect the overall defect concentration (as inferred from relative intensity changes in the Raman LO quasimode, in Figure 8). At least a portion of these defects function as electrically inactive trapping sites for hydrogen (as surmised from the absorption edge shifts with potential and thickness, in Figures 4 and 5). Some of these trapping sites slow, but do not completely suppress, hydrogen diffusion at ambient temperatures (as inferred from absorption edge shifts over days to weeks, in Figure 6). Other trapping sites likely present a higher barrier to hydrogen diffusion, so this portion of the incorporated hydrogen remains trapped for longer periods of time (as deduced from the leveling of the absorption edge shift after several weeks, and the different leveling values of E_g with different applied poten-

tials). Finally, trapping sites would remain as defects even after the hydrogen diffuses out of the sample (as supported by the constant relative intensity of the Raman LO quasimode with aging).

Quantitative assessments of defect concentrations, as well as studies to determine more precisely the nature of the hydrogen-related complexes that lead to donor behavior in ZnO electrodeposits, will be the focus of future investigations.

Acknowledgements

The authors would like to thank Y.H. Lee (Biology), M. Garcia and Dr. K. Nag (Biochemistry), and H. Gillespie and Dr. R. Mason (Earth Sciences) for the use of materials characterization facilities at Memorial University of Newfoundland. This work was supported by the Natural Sciences and Engineering Research Council of Canada, the Canada Foundation for Innovation, the Industrial Research and Innovation Fund, and Memorial University of Newfoundland.

References

- [1] Ü. Özgür, Ya. I. Alivov, C. Liu, A. Teke, M. A. Reshchikov, S. Dogan, V. Avrutin, S.-J. Cho, H. Morkoç, *J. Appl. Phys.* 98 (2005) 041301.
- [2] S. Taunier, J. Sicx-Kurdi, P. P. Grand, A. Chomont, O. Ramdani, L. Parissi, P. Panheleux, N. Naghavi, C. Hubert, M. Ben-Farah, J. P. Fauvaruque,

- J. Connolly, O. Roussel, P. Morgensen, E. Mahé, J. F. Guillemoles, D. Lincot, O. Kerrec, *Thin Solid Films* 480–481 (2005) 526.
- [3] I. M. Dharmadasa, J. Haigh, *J. Electrochem. Soc.* 153 (2006) G47.
- [4] A. Goux, T. Pauporté, J. Chivot, D. Lincot, *Electrochim. Acta* 50 (2005) 2239.
- [5] R. E. Marotti, P. Giorgi, G. Machado, E. A. Dalchiele, *Solar Energy Mater. Solar Cells* 90 (2006) 2356.
- [6] T. Pauporté, D. Lincot, *Electrochim. Acta* 45 (2000) 3345.
- [7] R. E. Marotti, D. N. Guerra, C. Bello, G. Machado, E. A. Dalchiele, *Solar Energy Mater. Solar Cells* 82 (2004) 85.
- [8] W. Schindler, J. Kirschner, *Phys. Rev. B* 55 (1997) R1989.
- [9] C. G. Van de Walle, J. Neugebauer, *Nature* 423 (2003) 626.
- [10] C. G. Van de Walle, *Phys. Rev. Lett.* 85 (2000) 1012.
- [11] S. F. J. Cox, E. A. Davis, S. P. Cottrell, P. J. C. King, J. S. Lord, J. M. Gil, H. V. Alberto, R. C. Vilao, J. Piroto Duarte, N. Ayres de Campos, A. Weidinger, R. L. Lichti, S. J. C. Irvine, *Phys. Rev. Lett.* 86 (2001) 2601.
- [12] N. H. Nickel, K. Fleischer, *Phys. Rev. Lett.* 90 (2003) 197402.
- [13] E. Burstein, *Phys. Rev.* 93 (1954) 632.
- [14] S. Peulon, D. Lincot, *J. Electrochem. Soc.* 145 (1998) 864.
- [15] T. Yoshida, D. Komatsu, N. Shimokawa, H. Minoura, *Thin Solid Films* 451–452 (2004) 166.
- [16] M. Izaki, T. Omi, *J. Electrochem. Soc.* 143 (1996) L53.
- [17] B. Canava, D. Lincot, *J. Appl. Electrochem.* 30 (2000) 711.
- [18] J. Lee, S. C. Nam, Y. Tak, *Korean J. Chem. Eng.* 22 (2005) 161.

- [19] D. Bizzotto, Cyclic voltammetry virtual instrument and libraries for use with National Instruments LabVIEW, 2006, <http://www.chem.ubc.ca/faculty/bizzotto/instrumentation.html>.
- [20] D. Schwarzenbach, LATCON: Program for the LS-refinement of Lattice Constants, Uni Lausanne, Switzerland, 1975.
- [21] D. Gal, Y. Mastai, G. Hodes, L. Kronik, J. Appl. Phys. 86 (1999) 5573.
- [22] Powder Diffraction File, Joint Committee on Powder Diffraction Standards, ASTM, Philadelphia, PA, 2003, Card 36-1451.
- [23] J.-S. Lee, J. Maier, J. Mater. Res. 20 (2005) 2101.
- [24] V. Srikant, D. R. Clarke, J. Appl. Phys. 81 (1997) 6357.
- [25] J. P. Enríquez, X. Mathew, Solar Energy Mater. Solar Cells 76 (2003) 313.
- [26] S. J. Jokela, M. D. McCluskey, K. G. Lynn, Physica B 340 (2003) 221.
- [27] M. Izaki, Y. Saijo, J. Electrochem. Soc. 150 (2003) C73.
- [28] P. Barquinha, E. Fortunato, A. Gonçalves, A. Pimentel, A. Marques, L. Pereira, R. Martins, Superlattices and Microstruct. 39 (2006) 319.
- [29] K. A. Alim, V. A. Fonoberov, A. A. Balandin, Appl. Phys. Lett. 86 (2005) 053103.
- [30] Z. Q. Chen, A. Kawasuso, Y. Xu, H. Naramoto, X. L. Yan, T. Sekiguchi, R. Suzuki, T. Ohdaira, Phys. Rev. B 71 (2005) 115213.
- [31] F. Decremps, J. Pellicer-Porres, A. M. Saitta, J. Chervin, A. Polian, Phys. Rev. B 65 (2002) 092101.
- [32] Y. Zhang, H. Jia, R. Wang, C. Chen, X. Luo, D. Yu, C. Lee, Appl. Phys. Lett. 83 (2003) 4631.

- [33] A. Janotti, C. Van de Walle, *J. Cryst. Growth* 287 (2006) 58.
- [34] M. K. Jayaraj, A. Antony, M. Ramachandran, *Bull. Mater. Sci.* 25 (2002) 227.
- [35] L.-Y. Chen, W.-H. Chen, J.-J. Wang, F. C.-N. Hong, Y.-K. Su, *Appl. Phys. Lett.* 85 (2004) 5628.
- [36] T. C. Damen, S. P. S. Porto, B. Tell, *Phys. Rev.* 142 (1966) 570.
- [37] L. Bergman, X.-B. Chen, J. Huso, J. L. Morrison, H. Hoeck, *J. Appl. Phys.* 98 (2005) 093507.
- [38] G. J. Exarhos, S. K. Sharma, *Thin Solid Films* 270 (1995) 27.
- [39] M. G. Wardle, J. P. Gross, P. R. Briddon, *Phys. Rev. Lett.* 96 (2006) 205504.

List of Table and Figure Captions

Table 1. Representative listing of average crystallite sizes (d) and corresponding band gap energies (E_g , ± 0.01 eV) for ZnO films with different thicknesses prepared at different deposition potentials. Average crystallite sizes were determined from broadening measurements of the (101) XRD Bragg reflections.

Fig. 1. XRD data for electrodeposits prepared at different applied potentials (a) indicate phase pure ZnO (JCPDS 36-1451)[22]. Peaks due to the stainless steel substrate are marked with an asterisk (*). Refined lattice constants are plotted as functions of thickness and deposition potential in (b). Refined values agree well with standard ZnO lattice constants (dotted lines). The resulting c/a ratios are compared with the standard value (dotted lines) in (c).

Fig. 2. SEM images of ZnO electrodeposits. In the early stages of growth (a-c, all at -0.90 V), crystallites are well separated, and their diameters grow with increasing charge passed: (a) 0.14 C and 350 nm thick, (b) 0.30 C and 400 nm thick, (c) 0.50 C and 500 nm. Potential also affects film growth: (d) -1.00 V, (e) -1.10 V, and (f) -1.20 V, each with a thickness of 0.9 ± 0.1 μm .

Fig. 3. Sample thickness increases monotonically with charge collected during deposition. The regions of shallower slope for more positive deposition potentials correlate with dominant radial, rather than vertical, growth of the ZnO crystallites. Deposits prepared at potentials ≤ -1.10 V involve mixed crystallite morphologies and show a steeper slope.

Fig. 4. Diffuse reflectance spectra (a,b) and their derivatives (c,d) show that the energy of the optical absorption edge decreases with increasing deposit thickness. Deposits prepared at more negative potentials exhibit wider reflectance transitions.

Fig. 5. Optical band gap energies, plotted as a function of film thickness, for films prepared at different deposition potentials. The typical bulk value is 3.33 eV, as indicated by the dotted line. Lines connecting data are provided merely as guides to the eye.

Fig. 6. Representative data showing that optical band gap energies decrease with sample aging time. The decay time of the absorption edge energy does not vary significantly with deposition potential. The lines connecting data points are provided merely as guides to the eye.

Fig. 7. Charge passed, during 10 minutes, in three different electrolytes over a range of potentials. All measurements were performed at 70°C.

Fig. 8. Representative Raman spectra of ZnO electrodeposits with (a) the same deposition potential (-1.00 V) but different thicknesses, and (b) comparable thickness (1 μm) prepared at different deposition potentials.

Deposition potential (V)	Film thickness (μm)	d (nm)	E_g (eV)
-0.90	0.35	43 ± 2	3.37
	0.40	59 ± 6	3.35
	0.50	54 ± 5	3.33
-1.00	0.60	39 ± 2	3.38
	0.75	43 ± 2	3.37
	0.90	46 ± 3	3.35
-1.10	1.0	44 ± 3	3.37
	1.1	38 ± 2	3.36
	1.8	44 ± 3	3.20
-1.20	0.80	38 ± 2	3.28
	1.7	39 ± 2	3.24
	2.1	42 ± 2	3.15

Table 1

Figure 1

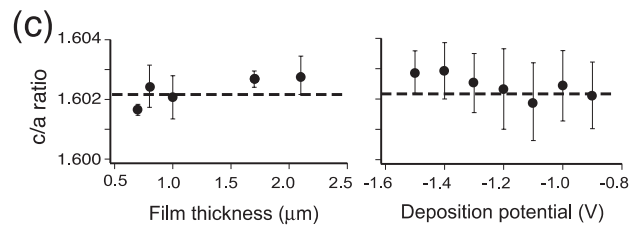
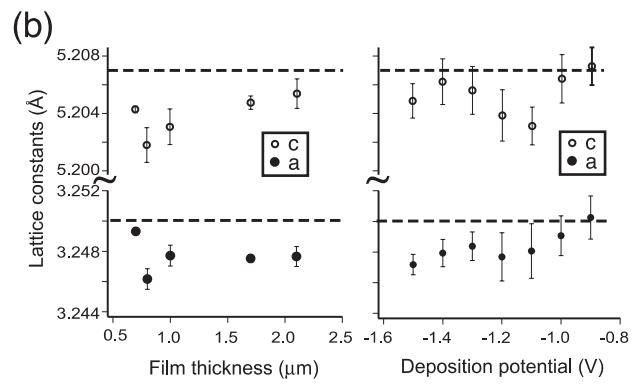
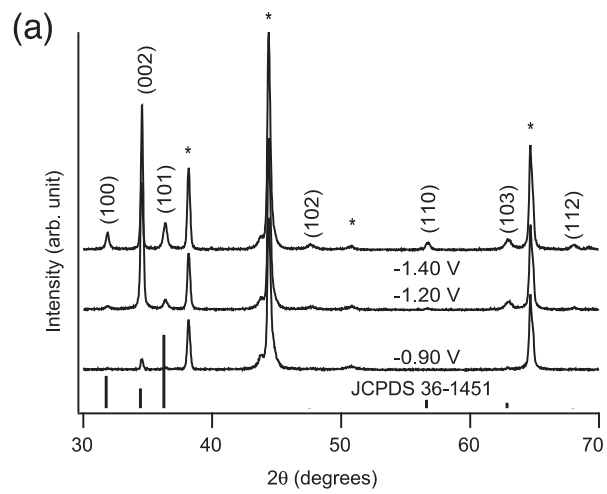


Figure 2
[Click here to download high resolution image](#)

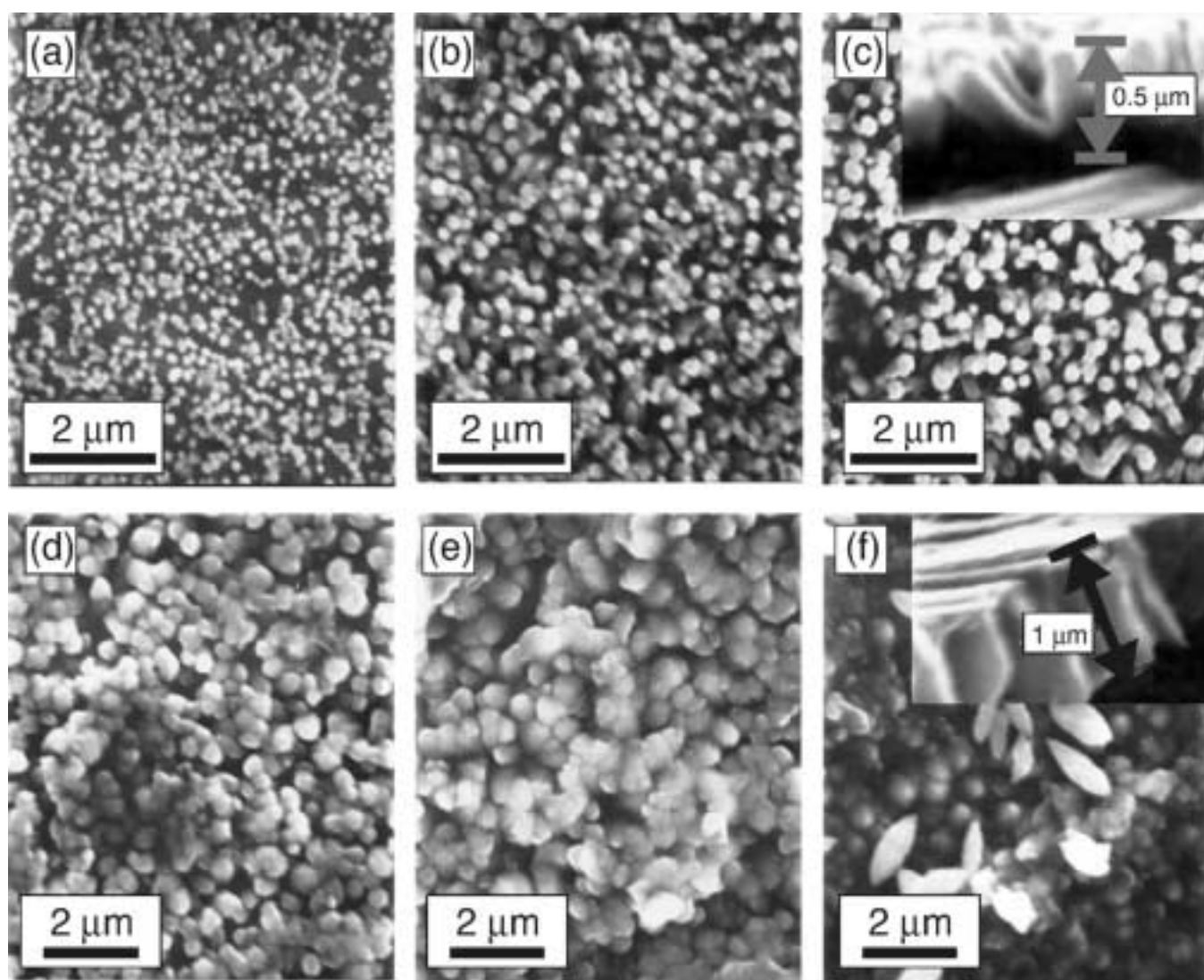


Figure 3

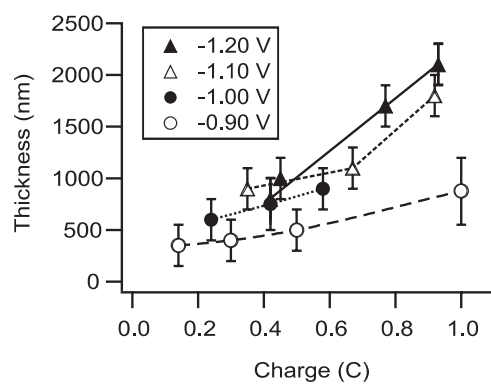


Figure 4

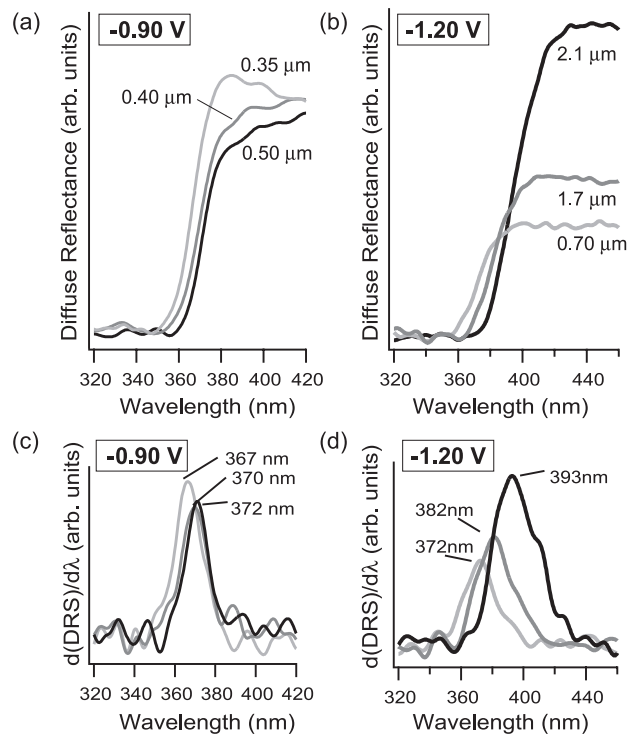


Figure 5
[Click here to download high resolution image](#)

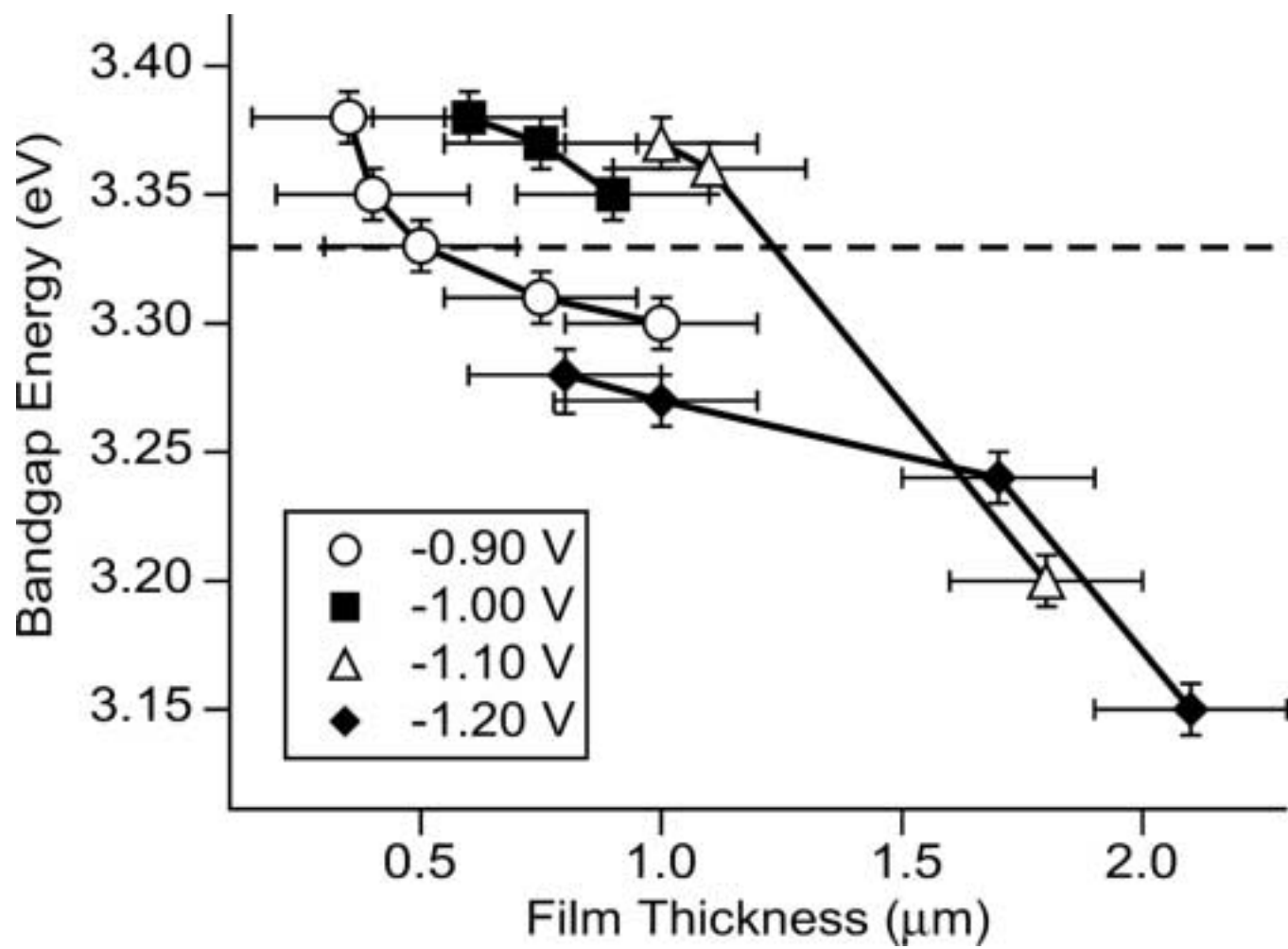


Figure 6
[Click here to download high resolution image](#)

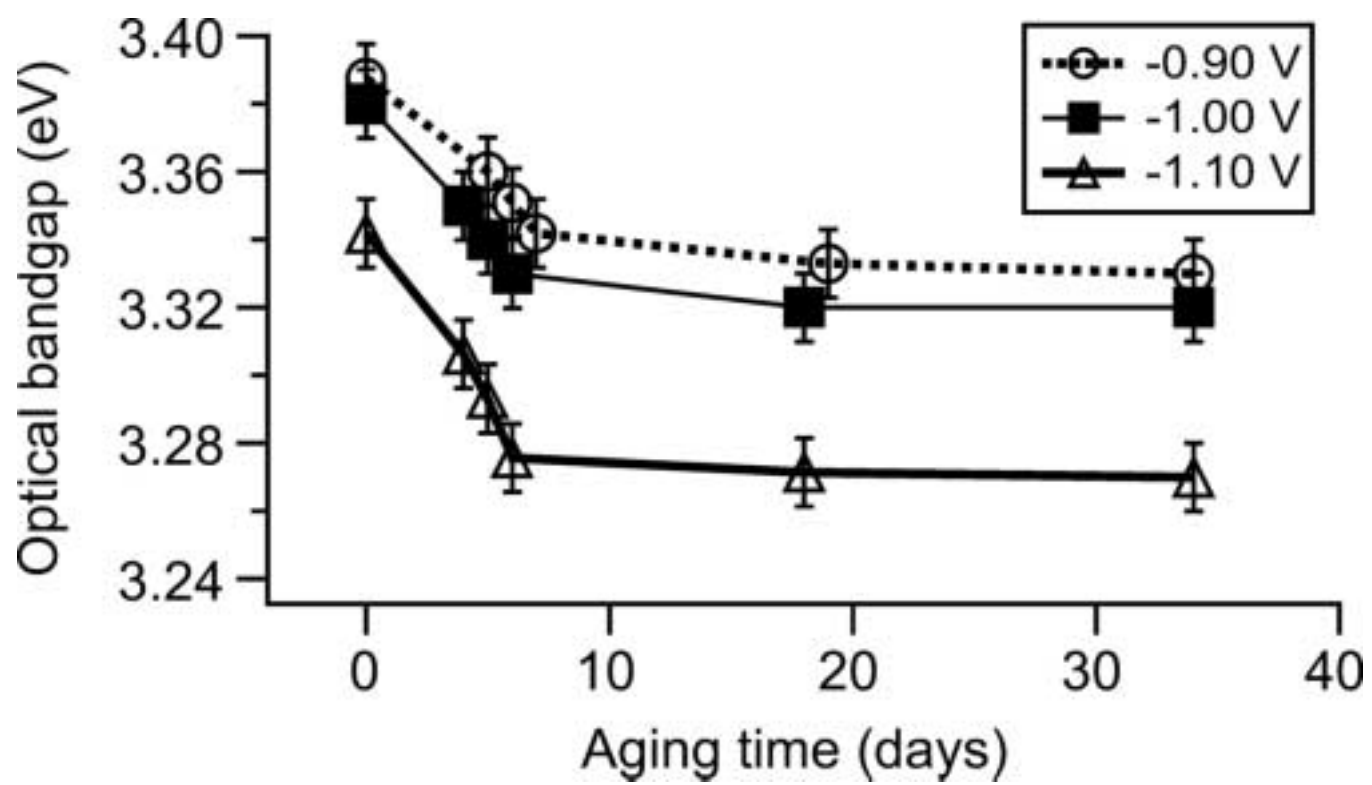


Figure 7
[Click here to download high resolution image](#)

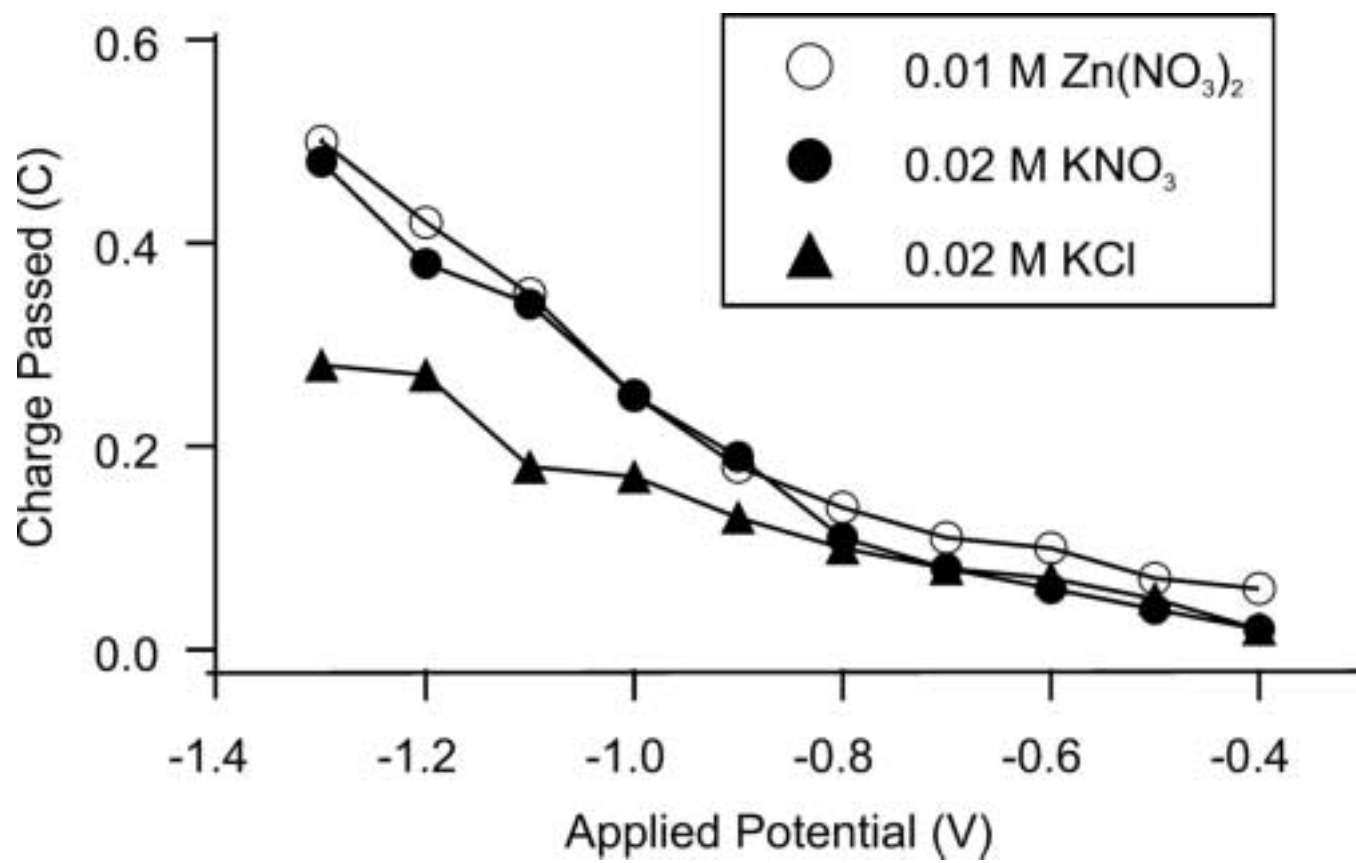


Figure 8
[Click here to download high resolution image](#)

